HHS Public Access

Author manuscript

NanoImpact. Author manuscript; available in PMC 2018 March 20.

Published in final edited form as:

NanoImpact. 2016 April ; 2: 70–81. doi:10.1016/j.impact.2016.07.001.

Effects of engineered nanomaterial exposure on macrophage innate immune function

Glen DeLoid[a,*], **Beatriz Casella**[a,b], **Sandra Pirela**[a], **Rose Filoramo**[a], **Georgios Pyrgiotakis**[a], **Philip Demokritou**[a], and **Lester Kobzik**[a,c]

[a]Center for Nanotechnology and Nanotoxicology, Department of Environmental Health, Harvard School of Public Health, Boston, MA, United States of America

[b]Faculty of Medicine, University of São Paulo, São Paulo, Brazil

[c]Department of Pathology, Brigham and Women's Hospital, Harvard Medical School, Boston, MA, United States of America

Abstract

Increasing use of engineered nanomaterials (ENMs) means increased human exposures. Potential adverse effects include those on the immune system, ranging from direct toxicity to impairment of defenses against environmental pathogens and toxins. Effects on lung macrophages may be especially prominent, because they serve to clear foreign materials like ENMs and bacterial pathogens. We investigated the effects of 4 hour exposures over a range of concentrations, of a panel of industry-relevant ENMs, including SiO_2, Fe_2O_3, ZnO, CeO_2, TiO_2, and an Ag/SiO2 composite, on human THP-1 macrophages. Effects on phagocytosis of latex beads, and phagocytosis and killing of *Francisella tularensis* (FT), as well as viability, oxidative stress and mitochondrial integrity, were measured by automated scanning confocal microscopy and image analysis. Results revealed some notable patterns: 1) Phagocytosis of unopsonized beads was increased, whereas that of opsonized beads was decreased, by all ENMs, with the exception of ZnO, which reduced both opsonized and unopsonized uptake; 2) Uptake of opsonized and unopsonized FT was either impaired or unaffected by all ENMs, with the exception of CeO_2, which increased phagocytosis of unopsonized FT; 3) Macrophage killing of FT tended to improve with all ENMs; and 4) Viability was unaffected immediately following exposures with all ENMs tested, but was significantly decreased 24 hours after exposures to Ag/SiO_2 and ZnO ENMs. The results reveal a complex landscape of ENM effects on macrophage host defenses, including both enhanced and reduced capacities, and underscore the importance of robust hazard assessment, including immunotoxicity assessment, of ENMs.

Keywords

macrophage; engineered nanomaterial; phagocytosis; innate immunity; host defense; Francisella tularensis

[*]corresponding author: Glen M. DeLoid, gdeloid@hsph.harvard.edu.

1. Introduction

A large and increasing variety of engineered nanomaterials (ENMs) are now common components of many industrial and consumer products [1–3], and more are being designed for novel diagnostic, antimicrobial, and therapeutic applications [4–11]. As such, the potential for workplace or environmental exposure to ENMs during their production and the life-cycle of products containing them, and for intentional exposure to therapeutic ENMs, is great [12–14]. The chemical compositions, small sizes and associated large surface-to-volume ratios of these materials suggest potential for harmful biological interactions [1,15–19]. Over the last decade the toxicity of ENMs has been studied extensively in a variety of *in vivo* and *in vitro* systems, and toxicity of metal oxide ENMs in particular has been often reported [2,20–22,14,23–29].

Most nanotoxicology studies have focused on direct toxicity, either physiological impairment or death *in vivo*, or various indicators of cytotoxicity *in vitro* [15,16,20–22,24–26,30]. Recent studies suggest the potential for indirect hazardous effects of ENMs through their interaction with the immune system. ENMs can alter innate and adaptive immune cells and processes, possibly causing impaired protection or disrupting immune homeostasis, leading to or exacerbating existing allergic and inflammatory conditions [31–33]. In this study we have focused on a key component of the innate immune system, the macrophage.

In the lung, the macrophage is the first line of defense against inhaled pathogens and particles, and also coordinates early inflammatory and immune responses as needed. Because it is strategically positioned and equipped to detect, engulf and destroy inhaled threats, the lung macrophage is also at high risk in inhalation exposures to ENMs. ENMs are readily and rapidly taken up by macrophages, and insoluble nano-sized particles can persist within macrophages for extended periods of time [34,35], raising the likelihood that ENM exposure could lead to both immediate and long-term macrophage dysfunction. Indeed, reported effects of ENM exposures on macrophages include changes in phagocytic function, as well as altered gene expression, cytokine secretion, reactive oxygen and nitrogen species production, and surface markers [36–40].

The few studies of ENM effects on macrophage function published to date have focused on one or two ENMs, and most have employed non-human macrophages [37–40], and effects on phagocytosis of opsonized beads or killed bacterial particles [36,38–40]. Given the growing variety of ENMs that pose potential exposure risks, and evidence from these early studies of ENM-induced macrophage dysfunction, there is a need for broader systematic study and development of efficient methods for screening ENM-induced macrophage dysfunction in relevant human cells. Moreover, since effective macrophage defense requires both phagocytosis and subsequent killing of inhaled pathogens, it is important to examine effects on both of these functions, using relevant live pathogenic bacteria. In addition, since opsonizing serum proteins are not normally present in alveolar fluid, macrophage function should be studied in the context of unopsonized as well as opsonized phagocytosis.

In the present study we have begun to address the needs outlined above. We employed human THP-1 macrophages, differentiated to maximize resemblance to primary lung

macrophages, to examine the effects of a panel of industry-relevant metal oxide ENMs, including SiO_2, Fe_2O_3, ZnO, CeO_2, TiO_2, and a composite of 10 percent Ag supported on SiO_2 particles (Ag/SiO2) [41,42]. We evaluated effects of test ENMs on key macrophage functions, including phagocytosis of both opsonized and unopsonized latex beads, and phagocytosis and killing of live *Francisella tularensis* (FT) using the live vaccine strain (LVS) of that pathogen. *Francisella tularensis* is a highly infectious Gram-negative intracellular pathogen, which causes the potentially fatal disease known as tularemia in humans and animals, and has been categorized as a category A select agent because of its potential for rapid dissemination [43,44]. These assessment were carried out using automated fluorescence scanning confocal microscopy and image analysis techniques, adapted from methods previously developed by the authors [45,46], as well as flow cytometry and lysis and CFU assays.

2. Materials and Methods

2.1. ENM powders and characterization

SiO_2, Fe_2O_3, CeO_2, and the composite Ag/SiO_2 ENM, consisting of 10 percent silver supported on SiO_2 particles, were produced by flame spray pyrolysis using the Harvard Versatile Engineered Nanomaterial Generation System (VENGES) as previously described [41,42,47]. TiO_2 and ZnO ENM powders were purchased from EVONIK (Essen, Germany), and Alfa Aesar (Ward Hill, MA, USA), respectively. ENMs were tested for endotoxin with a Limulus Amebocyte Lysate (LAL) chromogenic quantitation kit from ThermoFisher (Waltham, MA, USA) using 10 μg ml^{-1} suspensions of ENMs in water and following manufacturers instructions. Specific surface area, SSA, was determined by the nitrogen adsorption/Brunauer-Emmett-Teller (BET) method using a Micrometrics Tristar 3000 (Micrometrics, Inc., Norcross, GA, USA). Equivalent primary particle diameter, d_{BET}, was calculated, assuming spherical particles, as

$$d_{BET} = \frac{6}{SSA \times \rho_{\mathrm{p}}},$$

where ρ_{p} is the particle density, which was obtained for each particle from the densities of component materials, at 20°C, reported in the CRC handbook of Chemistry and Physics [48]. Particle crystal size and diameter was also determined by X-ray diffraction using a Scintag XDS2000 powder diffractometer (Scintag Inc., Cupertino, CA, USA), reported here as d_{XRD}.

2.2. ENM dispersal and characterization in suspension

Dispersions were prepared based on a protocol recently developed by the authors [49]. Sonication was performed in deionized water (DI H_2O) using the critical dispersion sonication energy (DSE_{cr}), which was determined as previously described for each ENM [49]. ENMs were dispersed at 5 mg cm^{-3} in 3 ml of solute in 15 ml conical polyethylene tubes using a Sonifer Cell Disruptor W200P probe sonicator (Heat Systems-Ultrasonics, Inc., Plainview, L.I., NY), calibrated by the calorimetric calibration method previously described [49,50]. Stock DI H_2O suspensions were then diluted to final concentrations in

either RPMI + 10% heat-inactivated FBS or PBS + 0.5% BSA and vortexed for 30 seconds. Dispersions were analyzed for hydrodynamic diameter (d_H), polydispersity index (PdI), zeta potential (ζ), and specific conductance (σ) by DLS using a Zetasizer Nano-ZS (Malvern Instruments, Worcestershire, UK). Effective density of particles and their formed agglomerates in suspension were determined using the Volume centrifugation method (VCM) as previously described[51]. Fate and transport modeling to determine mean delivered doses for each test ENM over the range of administered initial concentrations was performed using the distorted grid (DG) computational model recently published by the authors[52].

2.3. Biotinylation of latex beads

1 μm diameter green fluorescent latex beads were purchased from Life Technologies, and biotinylated as described previously [46]. Briefly, 100 mg of tissue culture grade BSA (Sigma Aldrich) dissolved in 15 ml of warm (37° C) PBS, and 50 mg of biotin-X-NHS (EMD Millipore, Billerica, MA) dissolved in 5 ml warm PBS, were vortexed together and incubated at room temperature for 1 hour, and twice dialyzed overnight at 4° C against 3 L of fresh PBS in two 10 ml aliquots in 12 ml capacity 7K MWCO Slide-A-Lyzer dialysis cassettes (ThermoFisher Scientific, Waltham, MA). Volume of recovered samples was adjusted to 10 ml by concentrating in 30K MWCO 15 ml capacity Amicon Ultra centrifugal filters units (EMD Millipore). Two samples of 20×10^{10} carboxylated 1 μm green fluorescent latex beads (Life Technologies) suspended in deionized water were centrifuged at 2,000 × g for 10 minutes, pellets washed and then resuspended, both times in 40 ml 0.1 M 2-(N morpholino) ethanesulfonic acid (MES) buffer (pH 6.0) (SantaCruz Biotechnology, Dallas, TX) containing 10 mg/ml of the water soluble carbodiimide (WSC) N-(3-Dimethylaminopropyl)-N′-ethylcarbodiimide (SantaCruz), and incubated for 1 hour at room temperature. Samples were then centrifuged at 4,200 × g for 20 minutes, pellets resuspended and washed in 20 ml 0.5 X PBS (diluted in deionized water), and resuspended in 10 ml deionized water (activated bead suspension).

Each 10 ml sample of activated bead suspension was combined with 10 ml of biotin-BSA solution and incubated while rocking overnight at room temperature. Samples were centrifuged at 4,200 × g for 20 minutes and pellets re-suspended and incubated at room temperature for 1 hour in 20 ml 0.5 X PBS with 40 mM glycine (to displace unreacted WSC/carboxyls through glycine's primary amine). Beads were then washed twice in 10 ml and finally resuspended in 5 ml of PBS containing 0.2% BSA and 0.01% sodium azide (final 4×10^{10} beads ml^{-1}), divided into 1 ml aliquots and stored at 4° C.

2.4. Preparation of bead suspensions

Beads were suspended at 2×10^9 beads/ml in 1.5 ml PBS, sonicated with a probe sonicator for 15 seconds, and diluted to 2×10^8 beads/ml in either RPMI + 0.3% BSA (unopsonized) or 10% Human AB serum (opsonized), and incubated at room temperature for 30 min prior to use to allow opsonization to occur.

2.5. Francisella tularensis suspensions

Francisella tularensis, subsp. holoarctica live vaccine strain (LVS) expressing green fluorescent protein (GFP) was generously provided by Dr. Larry S. Schlesinger (Ohio State University, Columbus, Ohio). Bacteria were grown to logarithmic phase in Modified Mueller-Hinton broth with tetracycline (10 μg ml^{-1}, selection agent) and aliquots stored at −80° C. Six days prior to experiments bacteria were thawed and streaked on Cystine Heart agar plates enriched with 1% chocolatized hemoglobin and containing 10 μg ml^{-1} tetracycline. A ~1 cm^3 sample of bacteria was collected from streak plates with an inoculating loop, suspended in 8 ml of PBS, and the suspension was filtered through a 5 μm syringe filter. A_{600} of a 1:5 dilution was measured and CFU ml^{-1} estimated from a standard A_{600}/CFU curve. The suspension was diluted to 5×10^8 CFU ml^{-1} stock for opsonized (RPMI + 10% human serum) or 1×10^9 ml^{-1} for unopsonized (RPMI + 0.3% BSA) uptake. Suspensions were incubated at room temperature for 30 min prior to use to allow opsonization to occur.

2.6. Macrophages

THP-1 monocytes were obtained from ATCC (Manassas, VA), and were cultured in RPMI supplemented with 10% heat-inactivated fetal bovine serum (FBS), 100 U ml^{-1} penicillin, 100 μg ml^{-1} streptomycin, and 10 mM HEPES. THP-1 monocytes were differentiated using the modified PMA protocol proposed by Diagneault et al. [53], which was shown to produces macrophages that closely resemble primary human macrophages in terms of morphology, phenotypic markers and function. Briefly, cells were resuspended at a 3.2×10^5 ml^{-1} in RPMI + 10% FBS containing 200 nM PMA, dispensed into 96-well black-walled imaging plates (BD, Franklin Lakes, NJ) at 8.0×10^5 cells per well or into 6-well cell culture plates (BD) at 1×10^6 cells per well, incubated for 3 days, washed with PBS, and incubated for an additional 4 days in RPMI + 10% FBS without PMA.

2.7. Cytotoxicity assay

Adherent THP-1 macrophages in 96-well microplate format were incubated at 37° C and 5% CO_2 for four hours with 100 μl (96-well plates) of ENM suspensions. For immediate cytotoxicity evaluation cells were then immediately incubated with 50 μl per well PBS + 2 μM Calcein AM (Life Technologies, Carlsbad, CA) + 4 μM Ethidium Homodimer 1 (Life Technologies) + 2 μg ml^{-1} Hoechst 33342 (Life Technologies) + 2.5 μg ml^{-1} HCS CellMask™ Blue stain (Life Technologies) at 37° C and 5% CO_2 for 40 minutes. For delayed (24 hour) toxicity evaluation, following the four hour ENM incubation, cells were washed twice with PBS, incubated overnight in RPMI + 10% FBS, and then stained as described above. At the end of the stain incubation, the stain mixture was replaced with PBS, and scanning confocal images were acquired immediately as described below.

2.8. ROS production and mitochondrial integrity assay

Adherent THP-1 macrophages in 96-well microplate format were pre-loaded with ROS probe by incubating in 50 μl per well of PBS + 10 μM CM-H2DCFDA (Life Technologies) at 37° C and 5% CO_2 for 30 minutes. Stain solution was then replaced with 100 μl of ENM suspensions and cells were incubated for four hours at 37° C and 5% CO_2. For evaluation of

immediate effects, cells were then washed with PBS and incubated with 50 μl per well PBS + 100 nM MitoTrackerRed-CMXRos (Life Technologies) + 2 μg ml^{-1} Hoechst 33342 (Life Technologies) + 2.5 μg ml^{-1} HCS CellMask™ Blue stain (Life Technologies) at 37° C and 5% CO_2 for 30 minutes. For 24 hour evaluation, following the four hour ENM incubation, cells were washed twice with PBS, incubated overnight in RPMI + 10% FBS, and then stained as described above. At the end of the stain incubation, the stain mixture was replaced with PBS, and scanning confocal images were acquired immediately as described below.

2.9. Latex bead phagocytosis assay

Cells were incubated for 4 hours at 37° C and 5% CO_2 with 100 μl (96-well plates) or 1.5 ml (6-well plates) of ENM suspensions, washed twice with PBS, incubated for 30 minutes with RPMI + 10% FBS +/− cytochalasin D (15 μM), incubated for 20 minutes with 50 μl (96-well) or 750 μl (6-well) of biotinylated bead suspensions to allow binding, washed twice with PBS, and incubated with RPMI + 10% FBS +/− cytochalasin D (15 μM) for an additional 30 minutes for internalization. Cells in 6-well plates were washed twice with cold PBS and processed for either flow cytometry or lysis and CFU counting as described below. Cells in 96-well plates were washed once with cold PBS, incubated at 4° C for 1 hour with 4 μg ml^{-1} AlexaFluor594-streptavidin (Life Technologies, Carlsbad, CA) in PBS + 1% BSA, washed twice with cold PBS, fixed with 4% formaldehyde at room temperature for 10 minutes, washed twice with PBS, incubated with 50 μl per well PBS + 2 μg ml^{-1} Hoechst 33342 (Life Technologies) + 2.5 μg ml^{-1} HCS CellMask™ Blue stain (Life Technologies) at room temperature for 1 hour, washed with PBS and stored in 200 μl per well PBS at 4°C prior to scanning.

2.10. Bacterial phagocytosis assay

Cells were incubated for 4 hours at 37° C and 5% CO_2 with 100 μl (96-well plates) or 1.5 ml (6-well plates) of ENM suspensions, washed twice with PBS, incubated for 30 minutes with RPMI + 10% FBS +/− cytochalasin D (15 μM), followed by incubation for 2 hours with 50 μl (96-well) or 750 μl (6-well) of FT suspension. Following phagocytosis, cells were washed twice with PBS and processed for scanning cytometry, flow cytometry or lysis and CFU counting. Cells for scanning cytometry were fixed with 4% formaldehyde at room temperature for 10 minutes, washed twice with PBS, incubated with 50 μl per well PBS + 2 μg ml^{-1} Hoechst 33342 (Life Technologies) + 2.5 μg ml^{-1} HCS CellMask™ Blue stain (Life Technologies) at room temperature for 1 hour, and washed twice with PBS before storage in 200 μl per well PBS at 4°C prior to scanning. Cells were processed for flow cytometry or lysis and CFU counting as described below.

2.11. Bacterial killing assay

Cells were incubated for 2 hours at 37° C and 5% CO_2 with 50 μl (96-well) or 750 μl (6-well) of FT suspension for phagocytosis, washed twice with PBS, incubated for 30 minutes with RPMI/10% FBS + 100 μg/ml gentamicin to kill external bacteria, washed twice with PBS, incubated for 4 hours at 37° C and 5% CO_2 with 100 μl (96-well plates) or 1.5 ml (6-well plates) of ENM suspensions, washed twice with PBS, incubated for an additional 18 hours in RPMI + 10% FBS, washed twice with PBS and processed for scanning cytometry, as described above, or for flow cytometry or lysis and CFU counting, as described below.

2.12. Scanning cytometry and analysis

Confocal fluorescence microscopy was performed using a BD Pathway 855 High-Content Bioimager with a 20× NA075 objective (Olympus), with laser auto-focus, 2×2 binning and flat field correction. Collapsed confocal stack (from Z-stack images at 1.5 μm intervals) were acquired using standard excitation, emission, and dichroic filters for green (Calcein AM, CM-H2DCFDA, GFP-expressing *F. tularensis*, green fluorescent beads), blue (Hoechst/CellMask Blue) and red (Ethidium Homodimer 1, MitoTrackerRed-CMXRos, AlexaFluor594) channels. Sufficient image fields were collected from triplicate wells to provide a minimum of 500 cells for quantitative analysis of each sample condition. Image analysis and quantification was performed using our custom MATLAB ® (The Mathworks, Natick, MA) software as previously described [45,46].

2.13. Flow cytometry

Cells were incubated for 20 minutes at 4° C in 2 ml per well cold PBS without Ca/Mg + 10 mM EDTA, gently lifted by cell scraper, and aspirates and two subsequent washes collected in in individual 15 ml conical tubes. Cells were fixed by addition of an equal volume of 4% formaldehyde and incubation at room temperature for 10 minutes, washed twice by centrifugation with PBS, resuspended in 0.5 ml per sample of PBS and transferred to flow tubes. Cells were analyzed using a BD Canto II flow cytometer (BD Biosciences, Sparks, MD). 10,000 cells were analyzed for each sample.

2.14. Lysis and CFU

Cells were lysed by incubation for 5 minutes at room temperature in 2 ml per well 0.1% SDS in PBS without Ca/Mg, followed by vigorous pipetting. Aspirates were diluted to 1:500,00 and 1:500,000 and 100 μl of each dilution was spread onto triplicate Cystine Heart agar + 1% chocolatized hemoglobin plates. Plates were incubated at 37° C for 48 hours, and colonies were counted manually.

3. Results

3.1. ENM characterization and dosimetry

Characterizations of ENM powders are shown in Table 1, and characterization of the corresponding suspensions in culture media (RPMI + 10% heat-inactivated FBS) are shown in Table 2. All ENMs formed agglomerates averaging between roughly 120 and 240 nm in diameter, with considerable polydispersity in most cases, particularly for the ZnO material. Zeta potential was negative for all suspended materials, consistent with corona formation by albumin and other serum proteins with predominantly anionic surfaces. Effective densities ranged between roughly 1.1 (slightly greater than media density) for Ag/SiO_2 and SiO_2, to approximately 2.1 for CeO_2. Effective mean delivered concentrations (over the 4 hour exposures) determined for each initial concentration of each ENM using the DG model, are presented in Table 3. At the highest initial concentration used (50 μg ml^{-1}) the effective delivered concentrations among the test ENMs ranged from nearly identical to the initial concentration (e.g. for Ag/SiO_2 and SiO_2 ENMs) to more than three times the initial concentration (for TiO_2). Analysis of ENM suspensions (10 μg ml^{-1}) for endotoxin

contamination by chromogenic LAL assay showed no endotoxin present (< 0.1 EU ml^{-1}) in any of the ENMs used.

3.2. Cytotoxicity of ENMs

To assess ENM toxicity we examined cell viability by fluorescent live/dead staining with calcein AM and ethidium homodimer-1. We also used fluorescent probes to assess oxidative stress (ROS production) and mitochondrial function, both immediately and 24 hours after four hour ENM exposures (Figure 1). No loss of viability was observed immediately after treatment (four hours) with any of the ENMs in our panel. At 24 hours after exposure, however, significant dose-dependent decreases in viability were observed for Ag/SiO_2 and ZnO ENM-treated cells. With the exception of Fe_2O_3, which caused modest cell death 24 hours after exposure at an intermediate concentration (administered concentration of 12.5 μg ml^{-1}, delivered concentration of 16.38 μg ml^{-1}), none of the other ENMs affected viability at 24 hours. Most ENMs caused minimal changes in ROS (as indicated by reduction of non-fluorescent CM-H2DCFDA to its fluorescent form) immediately or 24 hours after exposure, except at the lowest concentration, where a 25 – 50 percent increase was observed at 24 hours. One exception to this pattern was a significant decrease in ROS relative to control 24 hours after exposure with intermediate concentrations of Fe_2O_3 ENM. Changes in mitochondrial integrity, as measured by mitochondrial membrane potential-dependent uptake of fluorescent dye (MitoTrackerRed-CMXRos), followed patterns that nearly mirrored those observed for changes in ROS. Specifically, increased dye uptake (membrane potential) was observed in most cases 24 hours after exposure at the lowest concentration. However, significant decreases in mitochondrial potential were observed at higher concentrations of Fe_2O_3 and CeO_2 at both four and 24 hours, and of ZnO at four (but not 24) hours.

3.3. Effect of ENMs on phagocytosis of latex beads

To investigate the effect of ENM exposure on phagocytosis, THP-1 macrophages were treated with ENM suspensions for four hours prior to assessment of uptake of opsonized and unopsonized 1 μm fluorescent latex beads. Differential staining and quantification of external bound and internalized beads by fluorescence scanning cytometry and automated image analysis was performed, as described previously [45,46], and detailed in the methods section. The results of these studies are summarized in Figure 2. Because changes in uptake can result either from altered binding or internalization of particles, it is useful to differentiate between these two possible contributions. Since external bound and internalized beads were differentially labeled and enumerated in our assay, we were able to calculate total beads per cell (bound external + internal) as well as internalized beads per cell, and the percentage of total beads internalized. In general, exposure to ENMs resulted in a decrease in both total and internalized opsonized beads, and a decrease in both total and internalized unopsonized beads. However, in most cases, the differences between individual treatment measurements and controls did not reach statistical significance (by one-way ANOVA with Dunnett's test for multiple comparisons, Figure 2). Example fluorescence confocal images illustrating differential staining of external bound beads and reduced uptake after exposure to Ag/SiO_2 ENM are shown in Figure 3 a. With most ENMs, these changes were most pronounced at the lowest concentrations tested (3.125 – 6.25 μg ml^{-1}). An exception to this

pattern was observed with ZnO ENMs, which caused increased internalization of unopsonized beads at low concentrations, but decreased internalization at high concentrations. Although none of the differences in unopsonized beads internalized between mean control and individual concentration exposures with ZnO reached significance, correlation analysis revealed a significant dose-dependent decrease in internalization ($r = -.873$, $p = 0.023$). Otherwise the pattern observed with ZnO exposure was identical to that observed with the other ENMs, with a particularly sharp and statistically significant decrease in total and internalized opsonized beads. The percent of total beads internalized, also shown in Figure 2, provides further insight into the functional cause of changes in numbers of beads internalized per cell. For all ENMs but ZnO, exposure caused little change in percent internalization, suggesting that regardless of the number of particles bound, the fraction of those bound particles that were subsequently taken up was unchanged, and that observed changes in internalized beads per cell was primarily a result of altered recognition and binding of particles. In this respect, ZnO was a notable exception, causing a dramatic and statistically significant concentration-dependent reduction in percent internalization for both opsonized and unopsonized beads, suggesting an impairment by ZnO of the internalization machinery as the primary cause of reduced uptake. As discussed below in greater detail, the effects of ZnO and Ag/SiO_2 on phagocytosis may be related to the delayed cytotoxicity observed 24 hours after treatment with these ENMs, rather than a direct effect on phagocytic processes.

To explore whether similar results would be obtained using a different methodology, we used flow cytometry to evaluate the effects of Ag/SiO_2 ENM on macrophage function. The data show a statistically significant and marked reduction in phagocytosis of opsonized beads (as well as a trend to increase phagocytosis of unopsonized beads, though not statistically significant). The flow cytometry results, shown in figure 3 b-c, are consistent with those observed using the scanning cytometry approach. In cells exposed to Ag/SiO_2 ENM, the area under the higher intensity, right-shifted set of peaks, corresponding to cells containing one or more fluorescent beads, was substantially diminished, relative to untreated controls, although not as much as seen in cells treated with the positive control, the actin polymerization inhibitor cytochalasin-D (Figure 3 b). This corresponded to a 50% decrease relative to untreated controls in mean fluorescence for cells exposed at 50 $\mu g\ ml^{-1}$ Ag/SiO_2 (Figure 3 c), identical to the decrease observed by scanning cytometry for the same treatment (Figure 2).

3.4. Effects of ENMs on phagocytosis and killing of *Francisella tularensis*

Francisella tularensis (FT) is gram negative intracellular pathogen that causes the potentially fatal disease tularemia in humans and animals [43], and has been categorized as a category A select agent because of its potential for weaponization and dissemination [44]. Using the differential staining and scanning cytometry approach we examined the effect of ENM exposure on phagocytosis and killing of the live vaccine strain (LVS) of FT. For these experiments we employed a GFP-expressing clone of the bacterium, with indirect immunofluorescence staining to selectively label external bacteria. To assess effects on phagocytosis, THP-1 macrophages were exposed to ENMs prior to phagocytosis of opsonized or unopsonized bacteria. For assessment of bacterial killing, macrophages were

treated with ENM suspensions after phagocytosis to ensure equal uptake in all samples. The results of these studies are summarized in Figure 4. Sample confocal images illustrating differential staining of external bound FT are shown in Figure 5 a. Treatment with ZnO ENMs caused a striking dose-dependent reduction in total and internalized unopsonized FT, but only a modest reduction of the same for opsonized FT. Treatment with Ag/SiO_2 also impaired both opsonized and unopsonized phagocytosis of FT. All other ENMs (SiO_2, Fe_2O_3, CeO_2 and TiO_2) caused slight impairment of opsonized, but not of unopsonized FT phagocytosis. A notable exception was observed with CeO_2 ENM, which produced a significant dose-dependent increase in the number of internalized unopsonized FT per cell. Percent internalization was also significantly diminished after treatment with both Ag/SiO_2 and ZnO ENMs, suggesting that these ENMs impaired both binding and internalization. As discussed below, effects of ZnO and Ag/SiO_2 on FT phagocytosis may be related to the delayed cytotoxicity caused by these ENMs.

All ENMs appeared to produce modest improvement in killing of both opsonized and unopsonized FT, as indicated by decreased bacteria per cell at 24 hours (Figure 4). Although the trend was consistent among ENMs, statistically significant differences were observed only at the highest administered concentration (50 μg ml^{-1}) of Ag/SiO_2 and TiO_2. It should be noted that the effective delivered concentration of TiO_2 was three times greater than that of Ag/SiO2, and that therefore Ag/SiO_2 was more potent in eliciting this response than TiO2.

The effects of Ag/SiO_2 and CeO_2 ENMs on FT phagocytosis and killing were also examined by flow cytometry and by lysis and CFU assay. The flow cytometry results were generally consistent with those from scanning cytometry (Figure 5 b-d). CeO_2 ENM treatment sharply increased phagocytosis of unopsonized FT, especially at the lowest concentration (Figure 5 b), and Ag/SiO_2 ENM significantly decreased phagocytosis of both opsonized and unopsonized FT at the highest concentration tested (Figure 5 c), and produced a modest reduction in bacterial load at 24 hours. (Figure 5 d). Lysis and CFU results (Figure 5 e-g) were also generally consistent, but less pronounced, with CeO_2 ENM increasing phagocytosis (Figure 5 e) and improving killing of unopsonized FT (Figure 5 g), and Ag/SiO_2 ENM reducing phagocytosis of both opsonized and unopsonized FT at the highest concentration (Figure 5 e).

4. Discussion

The biological effects of ENMs are highly dependent upon intrinsic particle properties such as composition, size, shape, surface chemistry and extrinsic culture media properties such as ionic strength, which define agglomeration state [49,54–56]. Surprisingly, we observed broad similarities in the response patterns in this study among a compositionally diverse set of ENMs. Exposure to most ENMs tested impaired THP-1 phagocytosis of human serum-opsonized latex beads, but improved phagocytosis of unopsonized beads. In most cases the percentage of total beads associated with cells that were phagocytosed was unaffected, suggesting that the observed changes in phagocytosis were at least in part due to changes in binding of beads to cell surface receptors. Likewise, in the FT phagocytosis and killing assay, exposure to most ENMs resulted in reduced phagocytosis of opsonized FT and either

reduced or unchanged levels of phagocytosis of unopsonized FT. There was, again, no change in percent internalization. Finally, all ENMs in our panel, to at least some degree, improved killing of internalized FT at 24 hours.

The general decrease in phagocytosis of opsonized beads and FT observed here is also consistent with several previous studies described above [36–40]. It might be argued that macrophage over-filling by ENM particles was the cause. However, this would be inconsistent with the increased phagocytosis we observed for unopsonized beads, as well as the fact that the effect was typically observed at the lowest ENM concentration tested. Another possible mechanism for decreased phagocytosis of opsonized particles is decreased surface receptor availability resulting from internalization during receptor-bound ENM particles and agglomerates. Such “ligand-hijacking” is consistent with our finding that percent internalization was usually unchanged, suggesting a receptor defect or deficiency. Moreover the timing of our phagocytosis challenges immediately after ENM exposure would have limited the opportunity for cells to recycle or replenish endocytosed receptors. Receptor internalization has also been proposed by Kodali et. al as a possible mechanism for reduced phagocytosis following ENM exposure [40].

In this study we did not attempt to identify or quantify expression of the specific receptors involved in phagocytosis of beads or FT, or in ENM uptake. Additional studies along these lines may help us to better understand the difference between effects observed on opsonized and unopsonized uptake. It is likely, however, since we used pooled human serum as the opsonizing agent, that uptake of our opsonized beads and FT was mediated at least in part by the complement receptor (Cr) and the Fcγ receptor, whereas unopsonized beads and FT were more likely recognized and bound by scavenger receptors (SR) such as SR-A and MARCO [57], or by other non-specific receptors. It should also be noted that serum proteins, including complement and IgG, do not normally occur in alveolar fluid, and that true opsonization, in the sense of marking particles or pathogens for recognition by specific receptors, would therefore not occur. Thus, phagocytosis by alveolar macrophages *in vivo* probably occurs primarily through SR and other non-specific receptors.

It is also worth noting that in biological fluids, proteins are typically adsorbed onto the surface of ENMs to form protein coronas, which in turn play an important role in determining receptor type and mechanism of uptake, as well as subsequent intracellular transport and toxicity [58–63]. Since ENMs in our studies were suspended in media containing heat-inactivated FBS, it is likely that binding and uptake of ENMs was mediated by SR or non-specific receptors. Indeed, several recent studies have demonstrated a prominent role for scavenger receptors in uptake of ENMs by macrophages and epithelial cells [60–63]. Whereas depletion of SR during ENM uptake is consistent with the observed reduction in uptake of unopsonized FT, it would leave unexplained our findings of diminished binding and uptake of opsonized beads and FT, and of enhanced binding and uptake of unopsonized beads. Moreover, SRs comprise a diverse “superfamily” of receptors [64], and it is not unlikely that the specific SRs mediating ENM uptake differ from those mediating unopsonized bead and microbe uptake. Given this, ligand-hijacking would seem to be an implausible explanation for the general pattern of effects of ENM exposure on phagocytosis observed in the present study.

Although outcomes for most ENMs examined conformed to the pattern described above, there were notable exceptions. In particular, ZnO ENM exposure led to a dramatic dose-dependent reduction in phagocytosis of both opsonized and unopsonized beads, and near complete abrogation of phagocytosis of unopsonized FT, but only a slight reduction in uptake of opsonized FT. In addition, whereas most ENMs had no effect on percent internalization of either beads or FT, diminished uptake resulting from ZnO ENM exposure was accompanied by a significant and sharp reduction in percent internalization, suggesting an impairment of the associated cytoskeletal machinery. Part or all of these effects may be a consequence of cytotoxicity caused by ZnO ENM exposure. Although no loss of viability was observed immediately after exposure, severe and dose-dependent loss of viability was observed 24 hours after exposure, suggesting that although not detectable by our methods, cell death was underway, which one might easily imagine impacting other cell functions such as phagocytosis. Several studies have found that ENM exposure can lead to activation of inflammasomes, with activation of caspase-1, which in turn activates and leads to release of IL-1β, and which through action on other targets also initiates a type of programmed cell death known as pyroptosis [65–67]. It is possible then, that the severe dysfunction observed after ZnO ENM exposure was associated with this process, rather than any direct effects on phagocytic pathways. However, this still leaves unexplained the observation that opsonized phagocytosis of FT was not substantially impacted by ZnO exposure. It should also be noted that Ag/SiO_2 ENM, which caused delayed toxicity similar to that seen with ZnO, did not significantly impair uptake of unopsonized beads or FT, although its negative effects on opsonized bead and FT uptake may, as in the case of ZnO, may be a result of cellular derangements underway, but not manifested as frank cell death, until 24 hours after exposure.

Another notable exception to the pattern observed for most ENMs is that of CeO_2 ENM, which was the only ENM tested that caused a statistically significant dose-dependent increase in phagocytosis (of unopsonized FT by scanning cytometry assays ($r = 0.897$, $p = .0292$, Figure 4). Like most other ENMs, CeO_2 also appeared to improve killing of both opsonized and unopsonized FT by scanning cytometry, although this only reached statistical significance at the highest concentration tested for opsonized FT. Improved phagocytosis and killing of FT after exposure to CeO_2 ENM were also observed by both flow cytometry and cell lysis and CFU (Figure 5). The combination of increased uptake and killing of FT by CeO_2 ENM at concentrations that did not affect viability either immediately or 24 hours after exposure (Figure 1), suggests a possible novel therapeutic application for this ENM. Because of its unique autoregenerative free-radical scavenging properties, CeO_2 has been proposed as a nanotherapeutic agent for disorders associated with oxidative stress [68–71]. It is not clear from our data whether these reported antioxidant properties of CeO_2 ENMs contributed to the facilitation of FT uptake or killing observed in this study. Although ROS generation following CeO_2 ENM exposure was not pronounced, it did not differ substantially from that observed with other ENMs. Further work is required to explore the efficacy and mechanism of this potential therapeutic use for CeO_2 ENMs.

While oxidative stress (ROS production) is well known to be a precursor to cytotoxicity and genotoxicity generally, which could in turn affect innate immune functions, ROS production also plays an important role in killing of intracellular bacteria, including FT [72–75]. Indeed,

FT has been shown to downregulate host cellular ROS responses and to produce superoxide disumtases in order to provide protection against ROS within macrophages [73–75]. It is thus possible that changes in ROS production caused by ENM exposure could alter FT killing by macrophages. However, in the case of the Fe_2O_3 ENM tested here, which caused a significant decrease in ROS production, there was no associated statistically significant change in killing function. Additional studies are needed to determine whether the improvements in bacterial killing observed with some ENMs (Ag/SiO_2 and TiO_2) can be attributed to changes in ROS production in infected cells that were pre-treated with ENMs.

Finally, mass transport (sedimentation and diffusion) over time plays an important role in determining effective dose delivered to cells, and since toxicology is by nature comparative, it is imperative that colloidal characterization include relevant transport properties (agglomerate/particle size and effective density), and that analysis of particle kinetics by computational fate and transport modeling be performed to provide dose metrics needed to properly interpret dose responses [49,51,76]. Accordingly, dose responses have been presented here in terms of delivered dose (mean concentration at the bottom of the cell culture well over the duration of the exposure. It is worth noting that as a result of differences in transport properties among the suspended ENMs, the effective dose ranges tested also differed among the test ENMs in these studies.

5. Conclusion

In this study we have demonstrated that ENM exposure can significantly alter key macrophage functions in either a detrimental or potentially advantageous way. It is important that hazard evaluation of potentially airborne ENMs include assessment of macrophage function. Inhalation is the most likely route of accidental ENM exposure, and lung macrophages, which provide the first line of defense against inhaled pathogens and particles, not only lie in direct line of fire, but are disposed to take up and concentrate ENMs that reach the alveolar space. Moreover, it is important to note that phagocytosis and killing by macrophages can proceed by a variety of mechanisms and signaling pathways, depending on the nature of the pathogen or particle, as well as the specific proteins or opsonins present. This point is underscored by the differences between effects of ENMs on serum-opsonized and unopsonized phagocytosis of beads and FT observed in the present study. Furthermore, we have previously shown that even among different strains of *Staphylococcus aureus*, macrophage uptake appears to proceed via different signaling pathways [45]. Focus in future work should therefore be given to developing a robust, but practical panel of harmonized macrophage functional screening assays.

Acknowledgments

The authors thank Dr. Larry S. Schlessinger from Ohio State University for generously providing us with the GFP-expressing *Francisella tularensis*, live vaccine strain (LVS) used in this study.

Funding information

This research project was supported by the Science without Borders program of the CAPES Foundation, by NIEHS grant (ES-00002), and by the Center for Nanotechnology and Nanotoxicology at The Harvard School of Public Health. This work was performed in part at the Harvard Center for Nanoscale Systems (CNS), a member of the

National Nanotechnology Infrastructure Network (NNIN), which is supported by the National Science Foundation under NSF award no. ECS-0335765

References

1. Pirela SV, Sotiriou GA, Bello D, Shafer M, Bunker KL, Castranova V, et al. Consumer exposures to laser printer-emitted engineered nanoparticles: A case study of life-cycle implications from nano-enabled products. Nanotoxicology. 2015; 9:760–8. DOI: 10.3109/17435390.2014.976602 [PubMed: 25387251]
2. Pirela S, Molina R, Watson C, Cohen JM, Bello D, Demokritou P, et al. Effects of copy center particles on the lungs: a toxicological characterization using a Balb/c mouse model. Inhal Toxicol. 2013; 25:498–508. DOI: 10.3109/08958378.2013.806614 [PubMed: 23895351]
3. Xia T, Li N, Nel AE. Potential health impact of nanoparticles. Annu Rev Public Health. 2009; 30:137–50. DOI: 10.1146/annurev.publhealth.031308.100155 [PubMed: 19705557]
4. Pyrgiotakis G, Vasanthakumar A, Gao Y, Eleftheriadou M, Toledo E, DeAraujo A, et al. Inactivation of foodborne microorganisms using engineered water nanostructures (EWNS). Environ Sci Technol. 2015; 49:3737–45. DOI: 10.1021/es505868a [PubMed: 25695127]
5. Pyrgiotakis G, McDevitt J, Gao Y, Branco A, Eleftheriadou M, Lemos B, et al. Mycobacteria inactivation using Engineered Water Nanostructures (EWNS). Nanomedicine. 2014; 10:1175–83. DOI: 10.1016/j.nano.2014.02.016 [PubMed: 24632246]
6. Jain K, Mehra NK, Jain NK. Potentials and emerging trends in nanopharmacology. Curr Opin Pharmacol. 2014; 15:97–106. DOI: 10.1016/j.coph.2014.01.006 [PubMed: 24598376]
7. Key J, Leary JF. Nanoparticles for multimodal in vivo imaging in nanomedicine. Int J Nanomedicine. 2014; 9:711–26. DOI: 10.2147/IJN.S53717 [PubMed: 24511229]
8. Tong S, Fine EJ, Lin Y, Cradick TJ, Bao G. Nanomedicine: tiny particles and machines give huge gains. Ann Biomed Eng. 2014; 42:243–59. DOI: 10.1007/s10439-013-0952-x [PubMed: 24297494]
9. Pyrgiotakis G, Vedantam P, Cirenza C, McDevitt J, Eleftheriadou M, Leonard SS, et al. Optimization of a nanotechnology based antimicrobial platform for food safety applications using Engineered Water Nanostructures (EWNS). Sci Rep. 2016; 6:21073.doi: 10.1038/srep21073 [PubMed: 26875817]
10. Ma X, Wang Q, Rossi L, Ebbs SD, White JC. Multigenerational exposure to cerium oxide nanoparticles: Physiological and biochemical analysis reveals transmissible changes in rapid cycling Brassica rapa. NanoImpact. 2016; 1:46–54. DOI: 10.1016/j.impact.2016.04.001
11. Servin AD, White JC. Nanotechnology in agriculture: Next steps for understanding engineered nanoparticle exposure and risk. NanoImpact. 2016; 1:9–12. DOI: 10.1016/j.impact.2015.12.002
12. Pal AK, Watson CY, Pirela SV, Singh D, Chalbot M-CG, Kavouras I, et al. Linking Exposures of Particles Released From Nano-Enabled Products to Toxicology: An Integrated Methodology for Particle Sampling, Extraction, Dispersion, and Dosing. Toxicol Sci. 2015; 146:321–33. DOI: 10.1093/toxsci/kfv095 [PubMed: 25997654]
13. Sotiriou GA, Singh D, Zhang F, Chalbot M-CG, Spielman-Sun E, Hoering L, et al. Thermal decomposition of nano-enabled thermoplastics: Possible environmental health and safety implications. J Hazard Mater. 2016; 305:87–95. DOI: 10.1016/j.jhazmat.2015.11.001 [PubMed: 26642449]
14. Pirela SV, Lu X, Miousse I, Sisler JD, Qian Y, Guo N, et al. Effects of intratracheally instilled laser printer-emitted engineered nanoparticles in a mouse model: A case study of toxicological implications from nanomaterials released during consumer use. NanoImpact. 2016; 1:1–8. DOI: 10.1016/j.impact.2015.12.001 [PubMed: 26989787]
15. Krewski D, Acosta D, Andersen M, Anderson H, Bailar JC, Boekelheide K, et al. Toxicity testing in the 21st century: a vision and a strategy. J Toxicol Environ Health B Crit Rev. 2010; 13:51–138. DOI: 10.1080/10937404.2010.483176 [PubMed: 20574894]
16. Oberdörster G. Nanotoxicology: in vitro-in vivo dosimetry. Environ Health Perspect. 2012; 120:A13. author reply A13. doi: 10.1289/ehp.1104320 [PubMed: 22214547]

17. Grassian, VH., Haes, AJ., Mudunkotuwa, IA., Demokritou, P., Kane, AB., Murphy, CJ., et al. Environ Sci Nano. Vol. 3. The Royal Society of Chemistry; 2016. NanoEHS – defining fundamental science needs: no easy feat when the simple itself is complex; p. 15-27.
18. Konduru NV, Jimenez RJ, Swami A, Friend S, Castranova V, Demokritou P, et al. Silica coating influences the corona and biokinetics of cerium oxide nanoparticles. Part Fibre Toxicol. 2015; 12:31.doi: 10.1186/s12989-015-0106-4 [PubMed: 26458946]
19. Lu X, Miousse IR, Pirela SV, Moore JK, Melnyk S, Koturbash I, et al. In vivo epigenetic effects induced by engineered nanomaterials: A case study of copper oxide and laser printer-emitted engineered nanoparticles. Nanotoxicology. 2016; 10:629–39. DOI: 10.3109/17435390.2015.1108473 [PubMed: 26559097]
20. Bakand S, Hayes A, Dechsakulthorn F. Nanoparticles: a review of particle toxicology following inhalation exposure. Inhal Toxicol. 2012; 24:125–35. DOI: 10.3109/08958378.2010.642021 [PubMed: 22260506]
21. Demokritou P, Gass S, Pyrgiotakis G, Cohen JM, Goldsmith W, McKinney W, et al. An in vivo and in vitro toxicological characterisation of realistic nanoscale CeO_2 inhalation exposures. Nanotoxicology. 2013; 7:1338–50. DOI: 10.3109/17435390.2012.739665 [PubMed: 23061914]
22. Lu X, Miousse IR, Pirela SV, Melnyk S, Koturbash I, Demokritou P. Short-term exposure to engineered nanomaterials affects cellular epigenome. Nanotoxicology. 2015; :1–11. DOI: 10.3109/17435390.2015.1025115
23. Pirela SV, Miousse IR, Lu X, Castranova V, Thomas T, Qian Y, et al. Effects of Laser Printer-Emitted Engineered Nanoparticles on Cytotoxicity, Chemokine Expression, Reactive Oxygen Species, DNA Methylation, and DNA Damage: A Comprehensive in Vitro Analysis in Human Small Airway Epithelial Cells, Macrophages, and Lymphobla. Environ Health Perspect. 2015; doi: 10.1289/ehp.1409582
24. Watson C, Ge J, Cohen J, Pyrgiotakis G, Engelward BP, Demokritou P. High-throughput screening platform for engineered nanoparticle-mediated genotoxicity using CometChip technology. ACS Nano. 2014; 8:2118–33. DOI: 10.1021/nn404871p [PubMed: 24617523]
25. Yokel RA, Hussain S, Garantziotis S, Demokritou P, Castranova V, Cassee FR. The Yin: An adverse health perspective of nanoceria: uptake, distribution, accumulation, and mechanisms of its toxicity. Environ Sci Nano. 2014; 1:406–428. DOI: 10.1039/C4EN00039K [PubMed: 25243070]
26. Zhou EH, Watson C, Pizzo R, Cohen J, Dang Q, Ferreira de Barros PM, et al. Assessing the impact of engineered nanoparticles on wound healing using a novel in vitro bioassay. Nanomedicine (Lond). 2014; 9:2803–15. DOI: 10.2217/nnm.14.40 [PubMed: 24823434]
27. Konduru NV, Murdaugh KM, Sotiriou GA, Donaghey TC, Demokritou P, Brain JD, et al. Bioavailability, distribution and clearance of tracheally-instilled and gavaged uncoated or silica-coated zinc oxide nanoparticles. Part Fibre Toxicol. 2014; 11:44.doi: 10.1186/s12989-014-0044-6 [PubMed: 25183210]
28. Konduru NV, Murdaugh KM, Swami A, Jimenez R, Donaghey TC, Demokritou P, et al. Surface modification of zinc oxide nanoparticles with amorphous silica alters their fate in the circulation. Nanotoxicology. 2015
29. Cohen JM, Derk R, Wang L, Godleski J, Kobzik L, Brain J, et al. Tracking translocation of industrially relevant engineered nanomaterials (ENMs) across alveolar epithelial monolayers in vitro. Nanotoxicology. 2014; 8(Suppl 1):216–25. DOI: 10.3109/17435390.2013.879612 [PubMed: 24479615]
30. Setyawati MI, Tay CY, Chia SL, Goh SL, Fang W, Neo MJ, et al. Titanium dioxide nanomaterials cause endothelial cell leakiness by disrupting the homophilic interaction of VE-cadherin. Nat Commun. 2013; 4:1673.doi: 10.1038/ncomms2655 [PubMed: 23575677]
31. Wang X, Reece SP, Brown JM. Immunotoxicological impact of engineered nanomaterial exposure: mechanisms of immune cell modulation. Toxicol Mech Methods. 2013; 23:168–77. DOI: 10.3109/15376516.2012.757686 [PubMed: 23256453]
32. Smith MJ, Brown JM, Zamboni WC, Walker NJ. From immunotoxicity to nanotherapy: the effects of nanomaterials on the immune system. Toxicol Sci. 2014; 138:249–55. DOI: 10.1093/toxsci/kfu005 [PubMed: 24431216]

33. Roy R, Kumar S, Tripathi A, Das M, Dwivedi PD. Interactive threats of nanoparticles to the biological system. Immunol Lett. 2014; 158:79–87. DOI: 10.1016/j.imlet.2013.11.019 [PubMed: 24316409]
34. Lehnert BE. Pulmonary and thoracic macrophage subpopulations and clearance of particles from the lung. Environ Health Perspect. 1992; 97:17–46. Available: http://www.pubmedcentral.nih.gov/articlerender.fcgi?artid=1519537&tool=pmcentrez&rendertype=abstract. [PubMed: 1396454]
35. Lay JC, Bennett WD, Kim CS, Devlin RB, Bromberg PA. Retention and intracellular distribution of instilled iron oxide particles in human alveolar macrophages. Am J Respir Cell Mol Biol. 1998; 18:687–95. DOI: 10.1165/ajrcmb.18.5.2948 [PubMed: 9569239]
36. Sahu D, Kannan GM, Vijayaraghavan R. Size-dependent effect of zinc oxide on toxicity and inflammatory potential of human monocytes. J Toxicol Environ Health A. 2014; 77:177–91. DOI: 10.1080/15287394.2013.853224 [PubMed: 24555677]
37. Lin C-D, Kou Y-Y, Liao C-Y, Li C-H, Huang S-P, Cheng Y-W, et al. Zinc oxide nanoparticles impair bacterial clearance by macrophages. Nanomedicine (Lond). 2014; 9:1327–39. DOI: 10.2217/nnm.14.48 [PubMed: 24628689]
38. Liu R, Yin L, Pu Y, Li Y, Zhang X, Liang G, et al. The immune toxicity of titanium dioxide on primary pulmonary alveolar macrophages relies on their surface area and crystal structure. J Nanosci Nanotechnol. 2010; 10:8491–9. Available: http://www.ncbi.nlm.nih.gov/pubmed/21121358. [PubMed: 21121358]
39. Bancos S, Stevens DL, Tyner KM. Effect of silica and gold nanoparticles on macrophage proliferation, activation markers, cytokine production, and phagocytosis in vitro. Int J Nanomedicine. 2015; 10:183–206. DOI: 10.2147/IJN.S72580
40. Kodali V, Littke MH, Tilton SC, Teeguarden JG, Shi L, Frevert CW, et al. Dysregulation of macrophage activation profiles by engineered nanoparticles. ACS Nano. 2013; 7:6997–7010. DOI: 10.1021/nn402145t [PubMed: 23808590]
41. Demokritou P, Büchel R, Molina RM, Deloid GM, Brain JD, Pratsinis SE. Development and characterization of a Versatile Engineered Nanomaterial Generation System (VENGES) suitable for toxicological studies. Inhal Toxicol. 2010; 22(Suppl 2):107–16. DOI: 10.3109/08958378.2010.499385 [PubMed: 20701428]
42. Sotiriou GA, Diaz E, Long MS, Godleski J, Brain J, Pratsinis SE, et al. A novel platform for pulmonary and cardiovascular toxicological characterization of inhaled engineered nanomaterials. Nanotoxicology. 2012; 6:680–90. DOI: 10.3109/17435390.2011.604439 [PubMed: 21809902]
43. Santic M, Al-Khodor S, Abu Kwaik Y. Cell biology and molecular ecology of Francisella tularensis. Cellular Microbiology. 2010; :129–139. DOI: 10.1111/j.1462-5822.2009.01400.x [PubMed: 19863554]
44. Darling RG, Catlett CL, Huebner KD, Jarrett DG. Threats in bioterrorism. I: CDC category A agents. Emerg Med Clin North Am. 2002; 20:273–309. Available: http://www.ncbi.nlm.nih.gov/pubmed/12120480. [PubMed: 12120480]
45. DeLoid GM, Sulahian TH, Imrich A, Kobzik L. Heterogeneity in macrophage phagocytosis of Staphylococcus aureus strains: High-throughput scanning cytometry-based analysis. PLoS One. 2009; 4
46. Sulahian TH, Imrich A, Deloid G, Winkler AR, Kobzik L. Signaling pathways required for macrophage scavenger receptor-mediated phagocytosis: analysis by scanning cytometry. Respir Res. 2008; 9:59. [PubMed: 18687123]
47. Sotiriou GA, Watson C, Murdaugh KM, Darrah TH, Pyrgiotakis G, Elder A, et al. Engineering safer-by-design, transparent, silica-coated ZnO nanorods with reduced DNA damage potential. Environ Sci Nano. 2014; 1:144–153. DOI: 10.1039/C3EN00062A [PubMed: 24955241]
48. Haynes, WM. CRC Handbook of Chemistry and Physics. 92nd. Boca Raton, USA: Taylor & Francis; 2011.
49. Cohen J, Deloid G, Pyrgiotakis G, Demokritou P. Interactions of engineered nanomaterials in physiological media and implications for in vitro dosimetry. Nanotoxicology. 2013; 7:417–31. Available: http://www.ncbi.nlm.nih.gov/pubmed/22393878. [PubMed: 22393878]

50. Taurozzi JS, Hackley VA, Wiesner MR. Ultrasonic dispersion of nanoparticles for environmental, health and safety assessment–issues and recommendations. Nanotoxicology. 2011; 5:711–29. DOI: 10.3109/17435390.2010.528846 [PubMed: 21073401]
51. DeLoid G, Cohen JM, Darrah T, Derk R, Rojanasakul L, Pyrgiotakis G, et al. Estimating the effective density of engineered nanomaterials for in vitro dosimetry. Nat Commun. 2014; 5:3514.doi: 10.1038/ncomms4514 [PubMed: 24675174]
52. DeLoid GM, Cohen JM, Pyrgiotakis G, Pirela SV, Pal A, Liu J, et al. Advanced computational modeling for in vitro nanomaterial dosimetry. Part Fibre Toxicol. 2015; 12:32.doi: 10.1186/s12989-015-0109-1 [PubMed: 26497802]
53. Daigneault M, Preston Ja, Marriott HM, Whyte MKB, Dockrell DH. The identification of markers of macrophage differentiation in PMA-stimulated THP-1 cells and monocyte-derived macrophages. PLoS One. 2010; 5doi: 10.1371/journal.pone.0008668
54. Rivera Gil P, Oberdörster G, Elder A, Puntes V, Parak WJ. Correlating physico-chemical with toxicological properties of nanoparticles: the present and the future. ACS Nano. 2010; 4:5527–31. DOI: 10.1021/nn1025687 [PubMed: 20973573]
55. Pyrgiotakis G, Blattmann CO, Demokritou P. Real-Time Nanoparticle-Cell Interactions in Physiological Media by Atomic Force Microscopy. ACS Sustain Chem Eng. 2014; 2:1681–1690. DOI: 10.1021/sc500152g [PubMed: 25068097]
56. Pyrgiotakis G, Blattmann CO, Pratsinis S, Demokritou P. Nanoparticle-nanoparticle interactions in biological media by atomic force microscopy. Langmuir. 2013; 29:11385–95. DOI: 10.1021/la4019585 [PubMed: 23978039]
57. Arredouani M, Yang Z, Ning Y, Qin G, Soininen R, Tryggvason K, et al. The scavenger receptor MARCO is required for lung defense against pneumococcal pneumonia and inhaled particles. J Exp Med. 2004; 200:267–72. DOI: 10.1084/jem.20040731 [PubMed: 15263032]
58. Cedervall T, Lynch I, Lindman S, Berggård T, Thulin E, Nilsson H, et al. Understanding the nanoparticle-protein corona using methods to quantify exchange rates and affinities of proteins for nanoparticles. Proc Natl Acad Sci U S A. 2007; 104:2050–5. DOI: 10.1073/pnas.0608582104 [PubMed: 17267609]
59. Milani S, Bombelli FB, Pitek AS, Dawson KA, Rädler J. Reversible versus irreversible binding of transferrin to polystyrene nanoparticles: soft and hard corona. ACS Nano. 2012; 6:2532–41. DOI: 10.1021/nn204951s [PubMed: 22356488]
60. Fleischer CC, Payne CK. Secondary structure of corona proteins determines the cell surface receptors used by nanoparticles. J Phys Chem B. 2014; 118:14017–26. DOI: 10.1021/jp502624n [PubMed: 24779411]
61. Singh RP, Ramarao P. Cellular uptake, intracellular trafficking and cytotoxicity of silver nanoparticles. Toxicol Lett. 2012; 213:249–59. DOI: 10.1016/j.toxlet.2012.07.009 [PubMed: 22820426]
62. Shannahan JH, Podila R, Aldossari AA, Emerson H, Powell BA, Ke PC, et al. Formation of a protein corona on silver nanoparticles mediates cellular toxicity via scavenger receptors. Toxicol Sci. 2015; 143:136–46. DOI: 10.1093/toxsci/kfu217 [PubMed: 25326241]
63. Roy R, Parashar V, Chauhan LKS, Shanker R, Das M, Tripathi A, et al. Mechanism of uptake of ZnO nanoparticles and inflammatory responses in macrophages require PI3K mediated MAPKs signaling. Toxicol In Vitro. 2014; 28:457–67. DOI: 10.1016/j.tiv.2013.12.004 [PubMed: 24368203]
64. Zani IA, Stephen SL, Mughal NA, Russell D, Homer-Vanniasinkam S, Wheatcroft SB, et al. Scavenger receptor structure and function in health and disease. Cells. 2015; 4:178–201. DOI: 10.3390/cells4020178 [PubMed: 26010753]
65. Yang E-J, Kim S, Kim JS, Choi I-H. Inflammasome formation and IL-1β release by human blood monocytes in response to silver nanoparticles. Biomaterials. 2012; 33:6858–67. DOI: 10.1016/j.biomaterials.2012.06.016 [PubMed: 22770526]
66. Yang E-J, Choi I-H. Immunostimulatory effects of silica nanoparticles in human monocytes. Immune Netw. 2013; 13:94–101. DOI: 10.4110/in.2013.13.3.94 [PubMed: 23885223]

67. Kusaka T, Nakayama M, Nakamura K, Ishimiya M, Furusawa E, Ogasawara K. Effect of silica particle size on macrophage inflammatory responses. PLoS One. 2014; 9:e92634.doi: 10.1371/journal.pone.0092634 [PubMed: 24681489]

68. Narayanan KB, Park HH. Pleiotropic functions of antioxidant nanoparticles for longevity and medicine. Adv Colloid Interface Sci. 2013; 201-202:30–42. DOI: 10.1016/j.cis.2013.10.008 [PubMed: 24206941]

69. Colon J, Herrera L, Smith J, Patil S, Komanski C, Kupelian P, et al. Protection from radiation-induced pneumonitis using cerium oxide nanoparticles. Nanomedicine. 2009; 5:225–31. DOI: 10.1016/j.nano.2008.10.003 [PubMed: 19285453]

70. Niu J, Azfer A, Rogers LM, Wang X, Kolattukudy PE. Cardioprotective effects of cerium oxide nanoparticles in a transgenic murine model of cardiomyopathy. Cardiovasc Res. 2007; 73:549–59. DOI: 10.1016/j.cardiores.2006.11.031 [PubMed: 17207782]

71. Chen J, Patil S, Seal S, McGinnis JF. Rare earth nanoparticles prevent retinal degeneration induced by intracellular peroxides. Nat Nanotechnol. 2006; 1:142–50. DOI: 10.1038/nnano.2006.91 [PubMed: 18654167]

72. Lindgren H, Stenmark S, Chen W, Tärnvik A, Sjöstedt A. Distinct roles of reactive nitrogen and oxygen species to control infection with the facultative intracellular bacterium Francisella tularensis. Infect Immun. 2004; 72:7172–82. DOI: 10.1128/IAI.72.12.7172-7182.2004 [PubMed: 15557642]

73. Ma Z, Russo VC, Rabadi SM, Jen Y, Catlett SV, Bakshi CS, et al. Elucidation of a mechanism of oxidative stress regulation in Francisella tularensis live vaccine strain. Mol Microbiol. 2016; doi: 10.1111/mmi.13426

74. Melillo AA, Mahawar M, Sellati TJ, Malik M, Metzger DW, Melendez JA, et al. Identification of Francisella tularensis live vaccine strain CuZn superoxide dismutase as critical for resistance to extracellularly generated reactive oxygen species. J Bacteriol. 2009; 191:6447–56. DOI: 10.1128/JB.00534-09 [PubMed: 19684141]

75. Rabadi SM, Sanchez BC, Varanat M, Ma Z, Catlett SV, Melendez JA, et al. Antioxidant Defenses of Francisella tularensis Modulate Macrophage Function and Production of Proinflammatory Cytokines. J Biol Chem. 2016; 291:5009–21. DOI: 10.1074/jbc.M115.681478 [PubMed: 26644475]

76. Cohen JM, Teeguarden JG, Demokritou P. An integrated approach for the in vitro dosimetry of engineered nanomaterials. Part Fibre Toxicol. 2014; 11:20.doi: 10.1186/1743-8977-11-20 [PubMed: 24885440]

- We investigated the effects ENMs, including SiO_2, Fe_2O_3, ZnO, CeO_2, TiO_2, and Ag/SiO2, on human THP-1 macrophages.
- Phagocytosis and killing of *Francisella tularensis* (FT) were measured by scanning confocal microscopy and image analysis.
- Phagocytosis of unopsonized beads was increased, whereas that of opsonized beads was decreased, by most ENMs.
- FT uptake was either impaired or unaffected by all ENMs, except CeO_2, which increased phagocytosis of unopsonized FT.
- Macrophage killing of FT tended to improve with all ENMs;

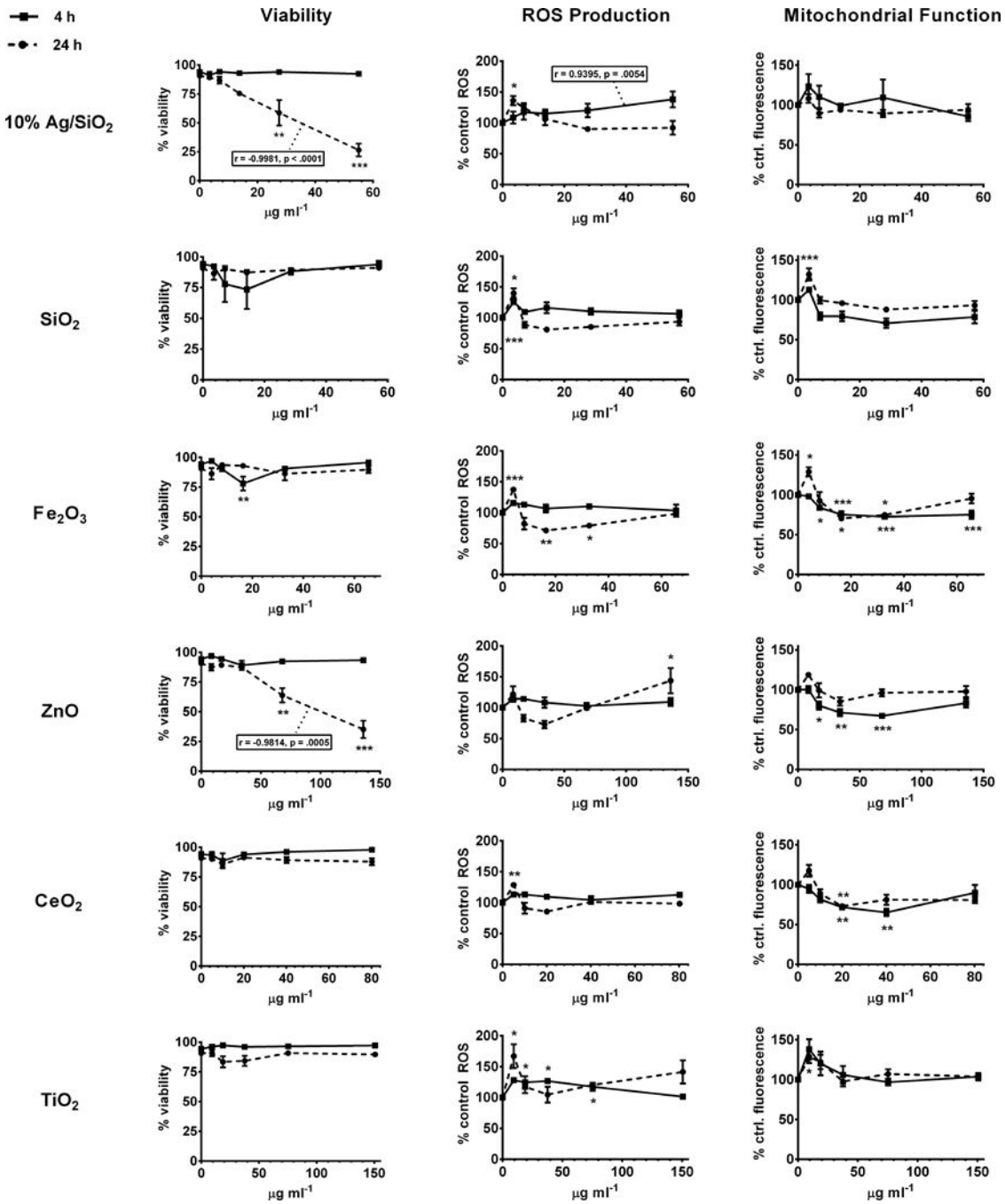

Figure 1.

NP panel cytotoxicity, mitochondrial function, and oxidative stress - scanning cytometry. Adherent PMA-matured THP-1 cells were incubated for 4 hours with indicated concentrations of nanoparticles, and stained either immediately or after wash and replacement with fresh media and overnight incubation. Cytotoxicity (% viability), ROS production (% control ROS) and mitochondrial function (% control fluorescence) are indicated for 4 h (immediately after exposure, solid lines) and 24 h (dashed lines) time

points. * = p<0.05; ** = p<0.01; ***=p<0.001; Statistically significant dose/response correlation coefficients (r) and P values are indicated in inset boxes.

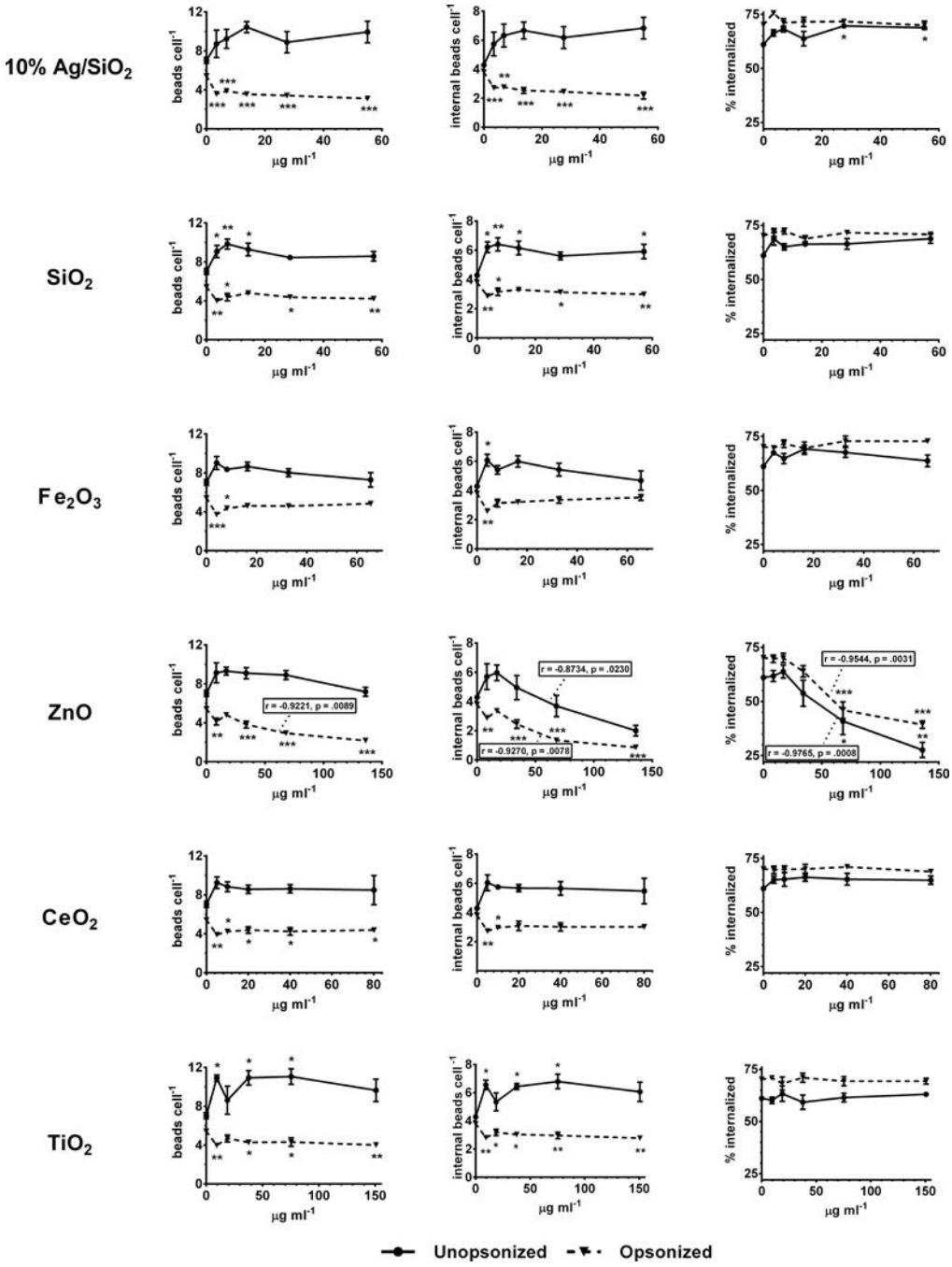

Figure 2.

NP panel polystyrene bead phagocytosis screen, scanning cytometry, dose response. Adherent PMA-matured THP-1 cells were incubated for 4 hours with indicated concentrations of nanoparticles prior to incubation with green fluorescent polystyrene beads. Total beads per cell, internal beads per cell, and percent internalized (100 × internal beads per cell/total beads per cell) are indicated for unopsonized (solid lines) and unopsonized (dashed lines) beads. * = $p<0.05$; ** = $p<0.01$; ***=$p<0.001$; Statistically significant dose/response correlation coefficients (r) and P values are indicated in inset boxes.

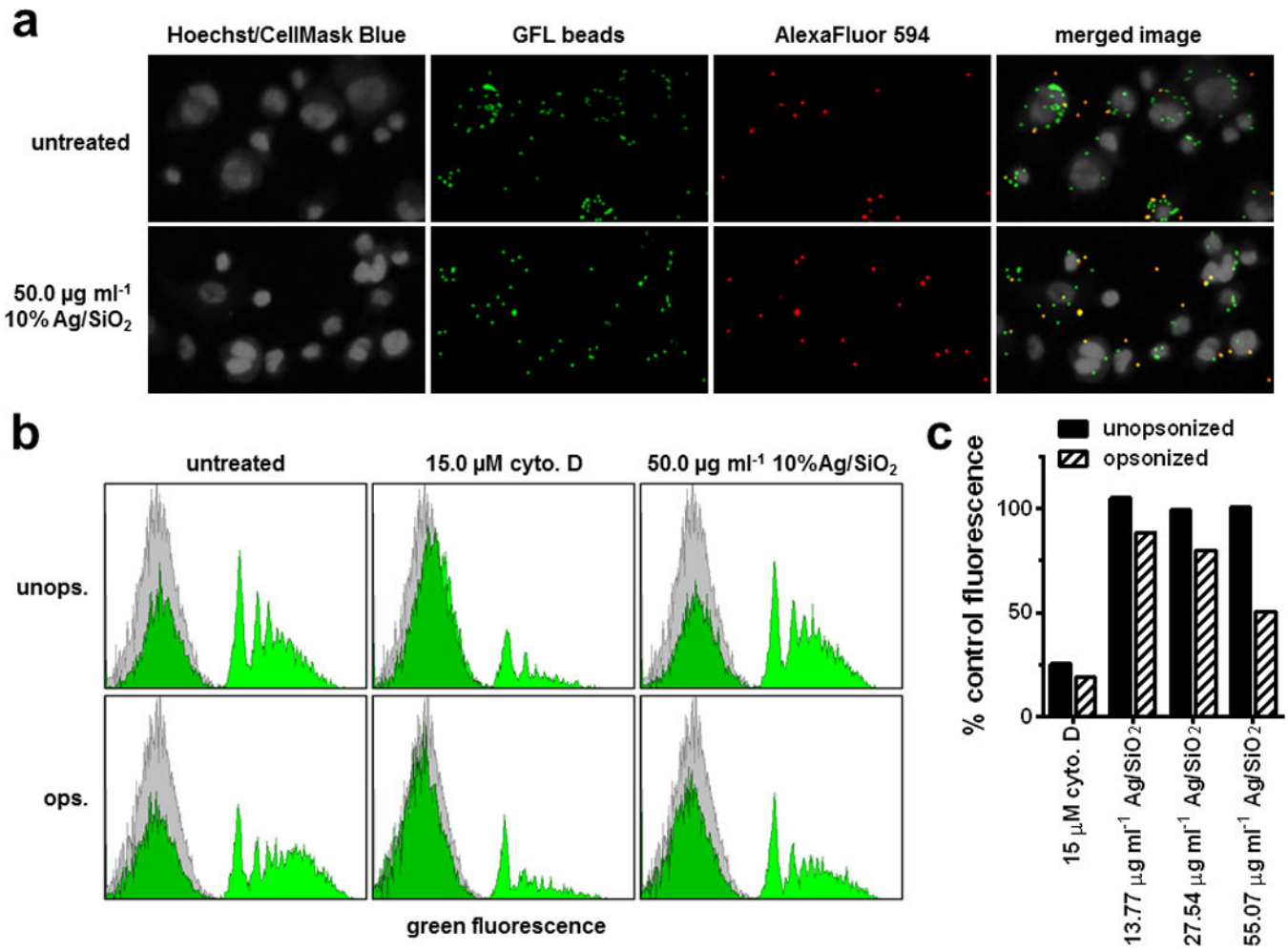

Figure 3.

Ag/SiO2 polystyrene bead phagocytosis, images and flow cytometry. Adherent PMA-matured THP-1 cells were incubated for 4 hours with indicated concentrations of 10% Ag/SiO2 prior to incubation with opsonized or unopsonized 1 μm biotinylated green fluorescent polystyrene beads. (a) representative confocal fluorescence images from latex bead phagocytosis experiments. All beads are seen in the green channel, and external beads, labeled with streptavidin-AlexaFluor 594, are seen in the red channel. (b) Representative cell fluorescence histograms from bead phagocytosis flow cytometry experiments. (c) quantification of flow cytometry (mean percent control fluorescence) for bead phagocytosis by cells treated with cytochalasin D control or indicated concentrations of Ag/SiO_2 ENMs.

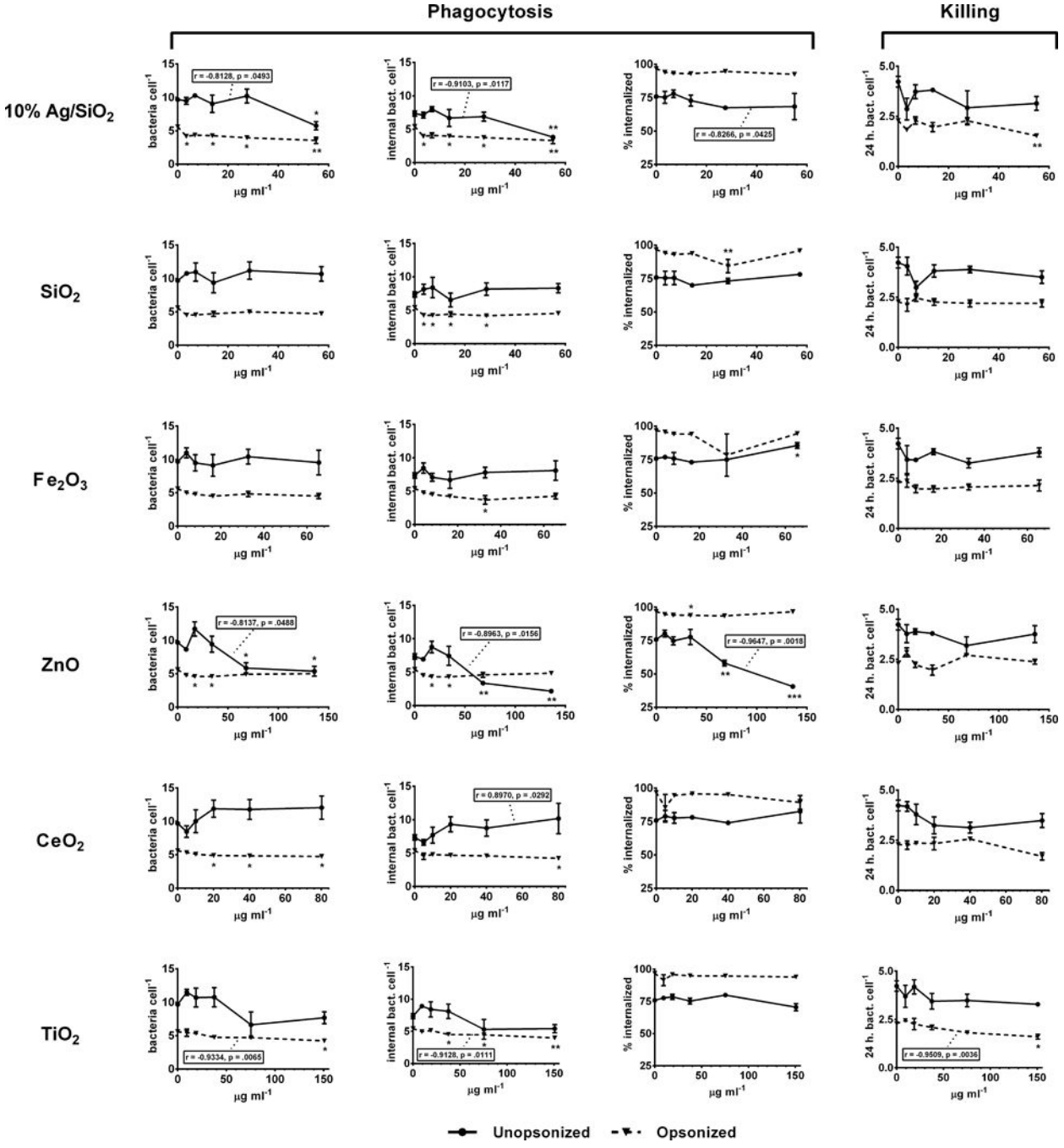

Figure 4.

NP panel *F. tularensis* phagocytosis and killing screen, scanning cytometry, dose response. For phagocytosis experiments, adherent PMA-matured THP-1 cells were incubated for 4 hours with indicated concentrations of ENMs prior to incubation for 2 hours with *F. tularensis*. For bacterial killing experiments cells were incubated for 2 hours with *F. tularensis*, then treated for 4 hours with ENM suspensions, washed, and incubated overnight (total 24 hours). Phagocytosis (total bacteria per cell, internal bacteria per cell, and percent internalized) and bacterial killing (bacteria per cell at 24 hours) are indicated for

unopsonized (solid lines) and unopsonized (dashed lines) beads. * = $p<0.05$; ** = $p<0.01$; ***=$p<0.001$; Statistically significant dose/response correlation coefficients (r) and P values are indicated in inset boxes.

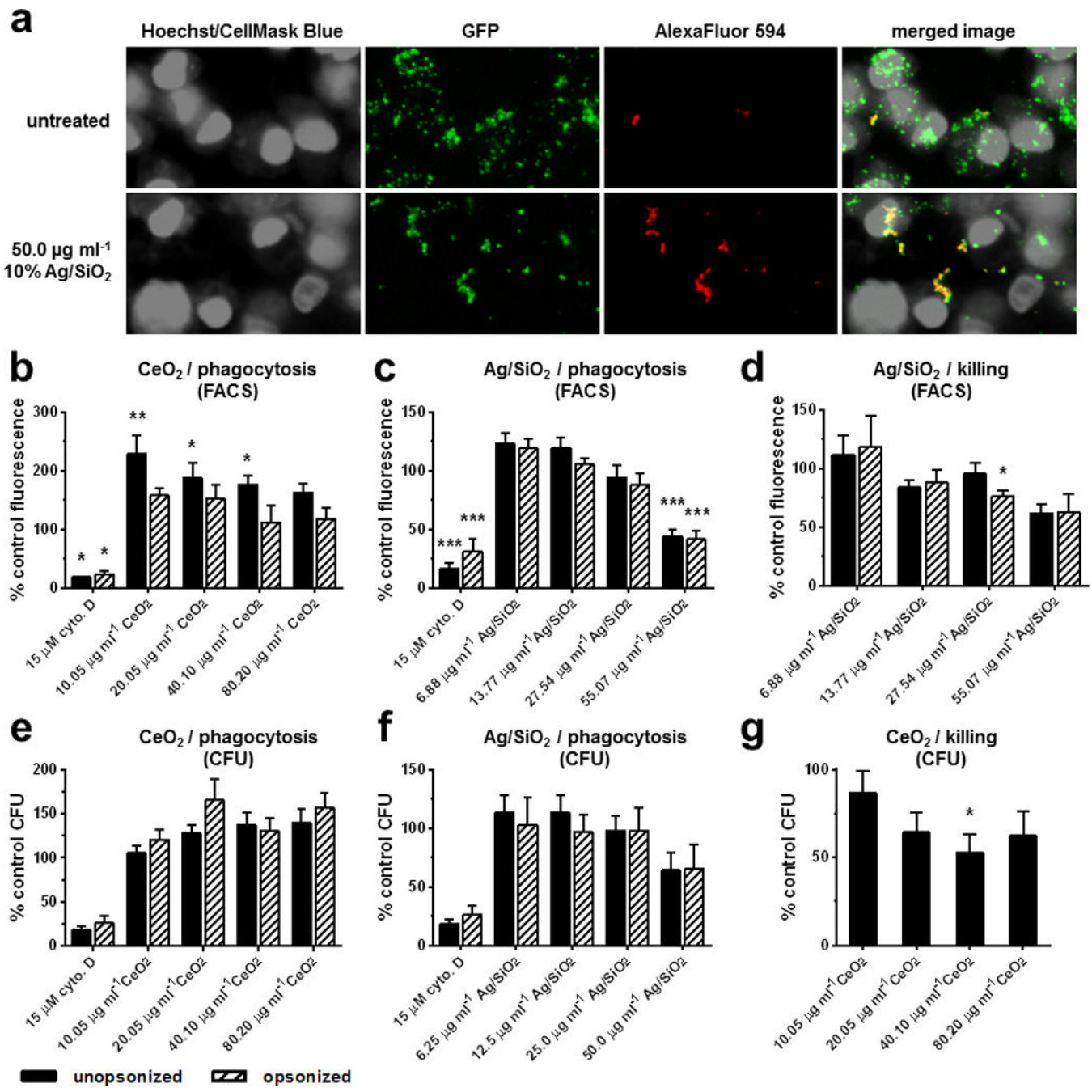

Figure 5.

F. tularensis phagocytosis and killing, scanning cytometry, images, flow cytometry and lysis/cfu. Adherent PMA-matured THP-1 cells were incubated for 4 hours with indicated concentrations of 10% Ag/SiO_2 or CeO_2 prior to or following incubation for 2 hours with *F. tularensis*. (a) representative confocal fluorescence images from FT phagocytosis experiments. All bacteria (GFP-expressing) are seen in the green channel, and external bacteria, labeled by indirect immunofluorescence staining with AlexaFluor 594, are seen in the red channel. (b, c) quantification of flow cytometry (mean percent control fluorescence) for FT phagocytosis by cells treated with cytochalasin D control or indicated concentrations

of either CeO_2 or Ag/SiO_2 ENMs. (d) quantification of flow cytometry for FT killing by cells treated with indicated concentrations of Ag/SiO_2 ENM. (e, f) quantification of cell lysis and CFU count experiments (percent control CFU) for FT phagocytosis by cells treated with indicated concentrations of CeO_2 or Ag/SiO_2 ENMs. (g) quantification of cell lysis and CFU count experiments for FT phagocytosis by cells treated with indicated concentrations of CeO_2 ENM. Results represent means ± standard deviation, N=3; * = $p<0.05$; ** = $p<0.01$; ***=$p<0.001$

Table 1

Materials Investigated, characterization of dry ENM powders

Material	***SSA*** **($m^2\ g^{-1}$)**	d_{BET} **(nm)**	d_{XRD} **(nm)**
VENGES Ag/SiO_2	375	6.7	6.9
VENGES SiO_2	231	11.8	NA
VENGES Fe_2O_3	131	8.7	NA
Alfa Aesar ZnO	17	63.0	22.3
VENGES CeO_2	144	5.4	9.5
Evonik TiO_2	50	28.4	33.0

Properties of ENM powder properties: *SSA*: specific surface area, d_{BET}: equivalent primary particle diameter, d_{XRD}: diameter by X-ray diffraction.

Table 2

Materials Investigated, colloidal characterization of suspensions in RPMI + 10% FBS.

Material	d_H (nm)	*PdI*	ζ (mV)	σ (mS cm^{-1})	ρ_{EV} (g cm^{-3})
VENGES Ag/SiO_2	179.2 ± 4.1	0.41 ± 0.05	−9.3 ± 1.3	12.7 ± 0.3	1.103 ± 0.004
VENGES SiO_2	182.7 ± 3.7	0.57 ± 0.03	−7.3 ± 1.0	12.4 ± 0.1	1.126 ± 0.002
VENGES Fe_2O_3	119.3 ± 1.2	0.44 ± 0.01	−7.5 ± 1.0	11.9 ± 0.7	1.715 ± 0.024
Alfa Aesar ZnO	219.8 ± 79.2	0.75 ± 0.28	−10.5 ± 2.4	12.4 ± 0.1	1.639 ± 0.019
VENGES CeO_2	127.8 ± 2.3	0.50 ± 0.01	−3.6 ± 5.0	11.2 ± 0.2	2.089 ± 0.114
Evonik TiO_2	234.9 ± 4.9	0.27 ± 0.01	−6.1 ± 4.8	11.4 ± 0.3	1.606 ± 0.008

ENM suspension properties: d_H: hydrodynamic diameter, *PdI*: polydispersity index, ζ: zeta potential, σ: specific conductance, ρ_{EV}: effective density measured by VCM. Values represent the mean (± standard deviation) of triplicate measurements.

Table 3

ENM administered and corresponding mean delivered concentrations.

	Administered concentration μg ml^{-1}				
	3.125	**6.25**	**12.5**	**25**	**50**
Material	**Mean delivered concentration μg ml^{-1}**				
VENGES Ag/SiO_2	3.44	6.88	13.77	27.54	55.07
VENGES SiO_2	3.57	7.14	14.29	28.59	57.17
VENGES Fe_2O_3	4.09	8.19	16.38	32.76	65.51
Alfa Aesar ZnO	8.50	17.00	34.00	68.00	136.0
VENGES CeO_2	5.01	10.03	20.05	40.10	80.20
Evonik TiO_2	9.42	18.84	37.68	75.35	150.70